Available online at www.sciencedirect.com
ScienceDirect
Journal of Power Sources 174 (2007) 832–837
JOURNAL OF POWER SOURCES
www.elsevier.com/locate/jpowsour

Short communication

# All solid battery with phosphate compounds made through sintering process

K. Nagata, T. Nanno *

*Technology Development Center, Matsushita Battery Industrial Co. Ltd., 1-1 Matsushita-cho, Moriguchi City, Osaka 570-8511, Japan*

Available online 3 July 2007

**Abstract**

Development of all solid ceramic batteries was investigated in our research. Sintering process was one of the facile ways to construct all ceramic batteries. But the drawback was that the heat treatment of an active material layer and a solid electrolyte layer in contact with each other induced the solid-state reaction between them, resulting in electrochemical deactivation of the interface. When phosphate solid electrolytes such as $Li_{1.3}Al_{0.3}Ti_{1.7}(PO_4)_3$ (LATP), and phosphate active materials such as $LiCoPO_4$ and $Li_3Fe_2(PO_4)_3$ were selected, both the solid electrolyte layer and the active material layers could be co-sintered without significant formation of new materials, and the resulted interfaces were found to be electrochemically active.


*Keywords:* Phosphate compound; All solid battery; Sintering process; Co-sintering; Interface

## 1. Introduction

All solid ceramic batteries have been paid attention because of their high reliabilities, potential durability against high temperature and safety.

Many dedicated work on sulfide solid electrolytes were reported [1–3], and some systems showed the ionic conductivity of $10^{-3}$ S cm$^{-1}$, which was comparable to the conventional organic liquid electrolyte. [4]. An electrochemical cell is usually fabricated by molding a pellet consisted of a positive electrode layer, a solid electrolyte layer and a negative electrode layer.

Other examples of batteries adopting inorganic solid electrolyte were thin-film lithium phosphorous oxynitride (LiPON) systems reported by Bates et al. [5]. But both systems suffer from either low output power or limited capacity besides sulfide electrolytes and LiPON are unstable to humidity in air. These problems make them difficult to fabricate all solid batteries for practical application.

On the other hand, the number of studies on all solid batteries adopting solid electrolytes of crystalline oxides is quite limited, though the oxide systems are stable in air [6–8]. The main reason is the difficulty in constructing interface between active materials and solid electrolytes [9]. That is, heat treatment of an active material layer and a solid electrolyte layer in contact with each other induces the solid-state reaction between them, which results in electrochemical deactivation of the interface.

When phosphate solid electrolytes such as $Li_{1.3}Al_{0.3}Ti_{1.7}(PO_4)_3$ (LATP), and phosphate active materials such as $LiCoPO_4$ and $Li_3Fe_2(PO_4)_3$ were selected, both the solid electrolyte layer and the active material layers could be co-sintered without significant formation of new materials, and the resulted interface were found to be electrochemically active. This work reports the electrochemical activities of the solid electrolyte/active material interface made thorough sintering process.

## 2. Experimental

### 2.1. Preparation of materials

LATP was prepared by the method reported by Aono et al. [10]. $LiCoPO_4$ was prepared by reacting stoichiometric amounts of $Co(OCOCH_3)_2{\cdot}4H_2O$, $Li_2CO_3$ and $(NH_4)_2HPO_4$ that were mixed and ground in an agate mortar and pestle. The mixture was calcined at 400 °C for 5 h to remove volatiles and 800 °C for 24 h in air with intermittent grinding. $Li_3Fe_2(PO_4)_3$ was prepared according to the method of Padhi et al. [11]. $LiCoO_2$ was prepared by heating the reaction mixture of $Li_2CO_3$ and $Co_3O_4$.

All the powder mixtures were ground to approximate average particle size of 1 μm by yttria stabilized zirconia balls having

* Corresponding author. Tel.: +81 6 6994 4630; fax: +81 6 6998 3179.
*E-mail address:* nanno.tetsuo@jp.panasonic.com (T. Nanno).

0378-7753/$ – see front matter © 2007 Elsevier B.V. All rights reserved.
doi:10.1016/j.jpowsour.2007.06.227

a diameter of 5 mm with *iso*-PrOH as a dispersive solvent. The powder was dried at 400 °C for 5 h in air.

The heat-treated powder was characterized by XRD (RINT 2500, Rigaku) with Cu Kα radiation by step scanning (0.02° $s^{-1}$) in the 2$\theta$ range of 10–80°, BET surface area (Micromeritech ASAP2010) and distribution of particle size (Horiba LA-920). Electrochemical performances of prepared materials were evaluated by constructing 2016 coin cell with Li foil as a reference and counter electrode, polypropylene separator and electrolyte (1.25 M $LiPF_6$ in ethylene carbonate/ethyl methyl carbonate 1:3). The electro active materials, acetylene black and polyvinylidene fluoride (PVdF) were mixed in weight ratio of 70:20:10 in an agate mortar and pestle. The cake obtained was pressed to make sheet of approximately 200 μm in thickness. The sheet was punched to 12 mm in diameter and used as an electrode.

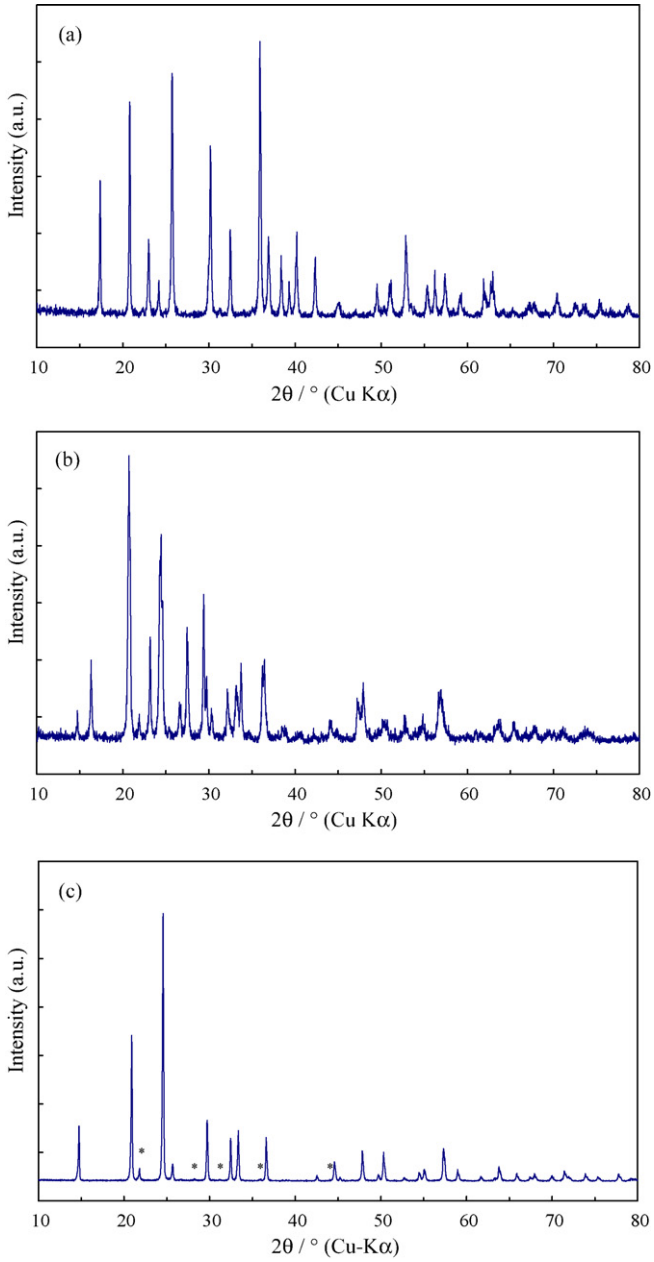


Fig. 1. XRD profiles of synthesized, (a) $LiCoPO_4$, (b) $Li_3Fe_2(PO4)_3$ (c) and LATP. *Show the peaks attributed to $AlPO_4$ phase.

### 2.2. Preparation of a laminated body (green chip)

The general procedure for the laminated body preparation was based on Ref. [12]. LATP powder prepared as above was mixed with *n*-butyl acetate to make dispersion. To this dispersion, polyvinyl butyral resin and benzyl butyl phthalate were added to obtain slurry of solid electrolyte. The slurry was formed into a solid electrolyte green sheet on a sheet of polyethylene terephthalate (PET) by the doctor blade process. The typical thickness of the green sheet was 25 μm.

The green sheet of $LiCoPO_4$ and $Li_3Fe_2(PO_4)_3$ were prepared by the same procedure described above; the typical thickness of the green sheets were 4 and 7 μm, respectively.

The green chip of $LiCoPO_4$ and LATP was made as following. On the green sheet of $LiCoPO_4$ was placed a piece of LATP green sheet, and then they were thermocompression-bonded (temperature of 80 °C; pressures of 13 MPa). The PET sheet on the LATP green sheet was removed and another piece of LATP green sheet was placed on the LATP green sheet and they were thermocompression-bonded as above. The same procedures were repeated for twenty times to obtain a laminated body of approximately 500 μm in thickness. The laminated body was cut into a size of 7 mm wide and 7 mm long to obtain green chip.

Green chips of other combination of materials were obtained in the same procedures as mentioned above.

### 2.3. Sintering of a green chip

A typical procedure for sintering a green chip is by sandwiching with alumina substrates and calcined at 400 °C for 5 h in air. Then, the chip was heated to 900–1000 °C at a rate of 1000 °C $h^{-1}$ and rapidly quenched to room temperature.

Gold was sputtered on the surface of an active material layer of the sintered chip as current collectors. A sintered chip was characterized by scanning electron microscopy (SEM, Hitachi S4500) and electron probe X-ray microanalysis (EPMA, JEOL

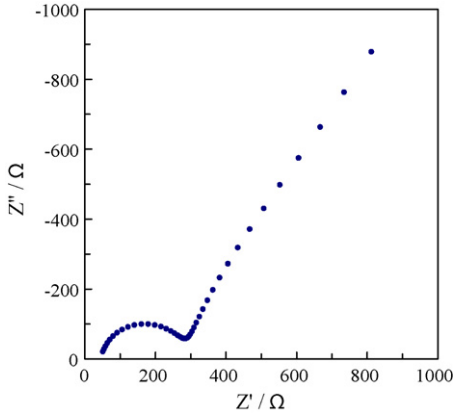


Fig. 2. Complex impedance plane plot for a sintered LATP pellet (15.2 mm in diameter, 0.972 mm in thickness) at 25 °C.

JXA-8900). Electrochemical performances of model cells were analyzed with a frequency response analyzer (Solartron 1260) with an electrochemical interface (Solartron 1287). The instruments were connected via GPIB interface to a computer and the data were analyzed by Zplot and CorrWare (Scribner Associates).

## 3. Results and discussion

### 3.1. Material characterization

The powder XRD profiles of synthesized $LiCoPO_4$, $Li_3Fe_2(PO_4)_3$ and LATP are represented in Fig. 1. The profiles of $LiCoPO_4$ and $Li_3Fe_2(PO_4)_3$ were in good agreement with the reported data [13,14]. The powder XRD of LATP showed an impurity $AlPO_4$ phase as discussed in Ref. [15].

Ionic conductivity of LATP was determined by impedance analysis of a sintered LATP chip. The impedance spectrum of LATP is shown in Fig. 2. The ionic conductivity was found to be $6.1 \times 10^{-4}$ S cm$^{-1}$, which was comparable to the reported value [10].

The charge and discharged performance of $LiCoPO_4$, $Li_3Fe_2(PO_4)_3$ and LATP are presented in Fig. 3a–c, respectively. $LiCoPO_4$ showed capacity of 136 mAh g$^{-1}$ that was comparable to the best value reported so far [16]. Irreversible capacity of 23 mAh g$^{-1}$ was observed in first discharge.

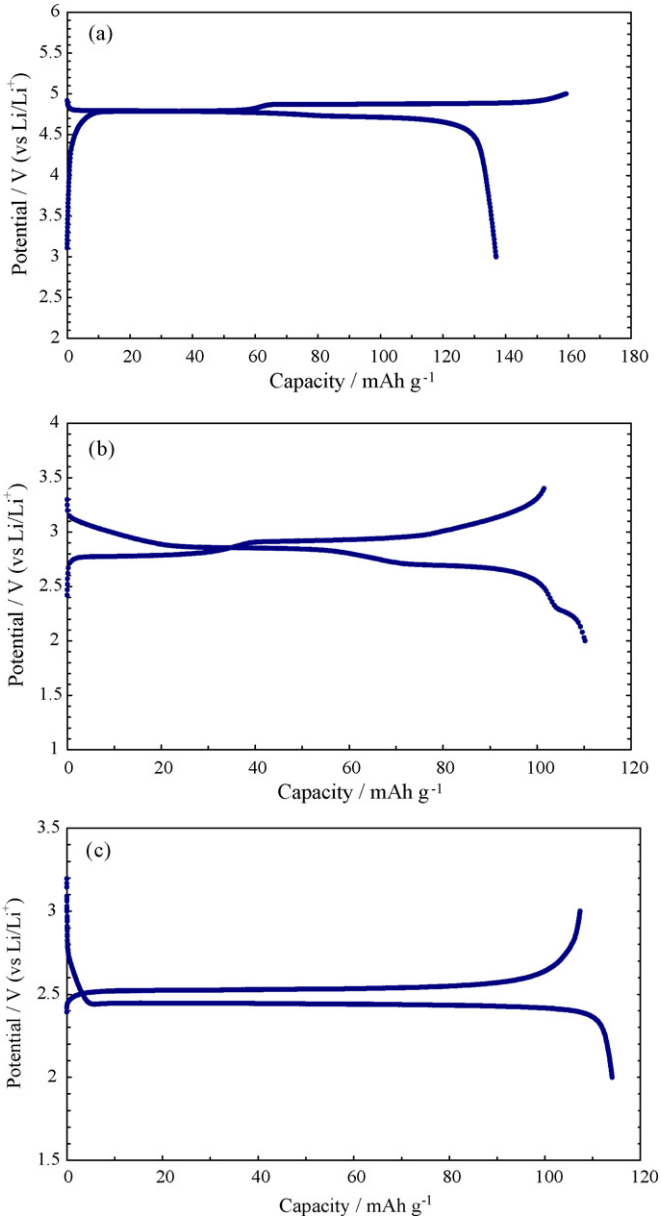


Fig. 3. The first charge–discharge curves for (a) $LiCoPO_4$ (cycled between 3 and 5.0 V at 1.1 mA g$^{-1}$), (b) $Li_3Fe_2(PO_4)_3$ (cycled between 2 and 3.4 V at 1.1 mA g$^{-1}$) and (c) LATP (cycled between 2 and 3 V at 5.9 mA g$^{-1}$).

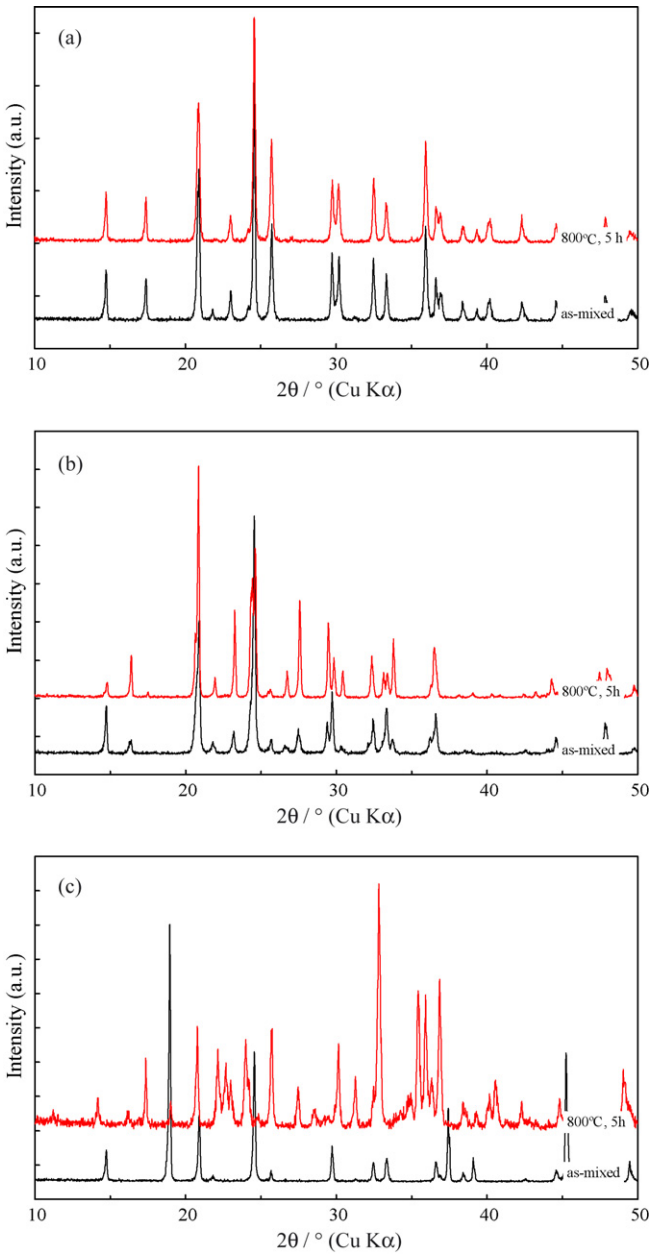


Fig. 4. XRD profiles of (a) $LiCoPO_4$/LATP, (b) $Li_3Fe_2(PO_4)_3$/LATP and (c) $LiCoO_2$/LATP mixtures before and after heat treatment. The powder mixtures were pelletized before heat treatment, pulverized after heat treatment with agate mortar and pestle for XRD measurements.

The Li insertion into $Li_3Fe_2(PO_4)_3$ occurred in two separate intercalation plateaus. The Li insertion capacity was 110 mAh $g^{-1}$, which was comparable to the value of 128 mAh $g^{-1}$ if all $Fe^{3+}$ could be reduced to $Fe^{2+}$. The electrochemical performances of $Li_3Fe_2(PO_4)_3$ were in good agreement with previous report [17]. The LATP showed 114 mAh $g^{-1}$ of Li insertion capacity, which was comparable to the value of 119 mAh $g^{-1}$ if all $Ti^{4+}$ could be reduced to $Ti^{3+}$ [18].

### 3.2. Co-sintering of active materials and a solid electrolyte

Co-sintering of electro active material with solid electrolyte was performed by taking equal mass of active material powder and LATP powder and heated at 800 °C for 5 h in air. In Fig. 4a–c are shown XRD profiles of powder mixture and heat-treated powders. As for $LiCoPO_4$/LATP and $Li_3Fe_2(PO_4)_3$/LATP, relative peak intensities changed with heat treatment because of the growth of crystallites, but no new peek was detected by heat treatment. On the other hand, new peeks were detected in XRD profile of $LiCoO_2$ and LATP by the heat treatment. The new peaks were attributed to $LiCoPO_4$ and other unknown phase. The results show that $LiCoPO_4$/LATP and $Li_3Fe_2(PO_4)_3$/LATP can be co-sintered without solid-state reactions.

### 3.3. Characterization of sintered chips

Figs. 5 and 6 show cross-section view of $LiCoPO_4$/LATP chip and $Li_3Fe_2(PO_4)_3$/LATP chip, respectively. As for a

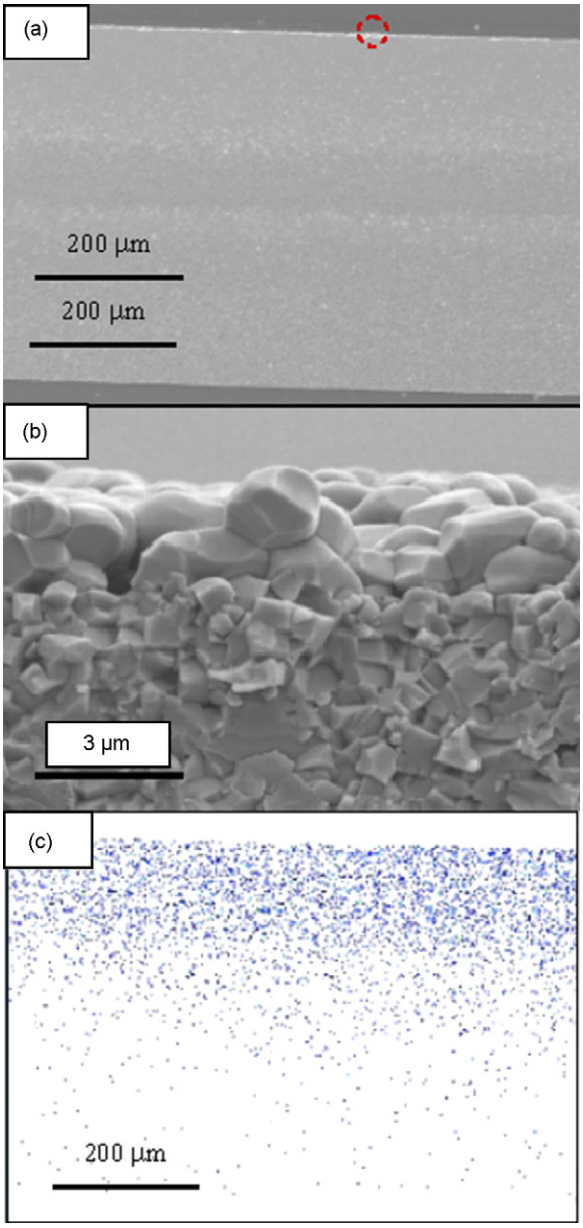


Fig. 5. Cross-section view of sintered $LiCoPO_4$/LATP chip. (a) A SEM image, (b) an enlargement of the interface at the circle of (a) and (c) an EPMA cobalt map. Maximum sintering temperature was 900 °C.

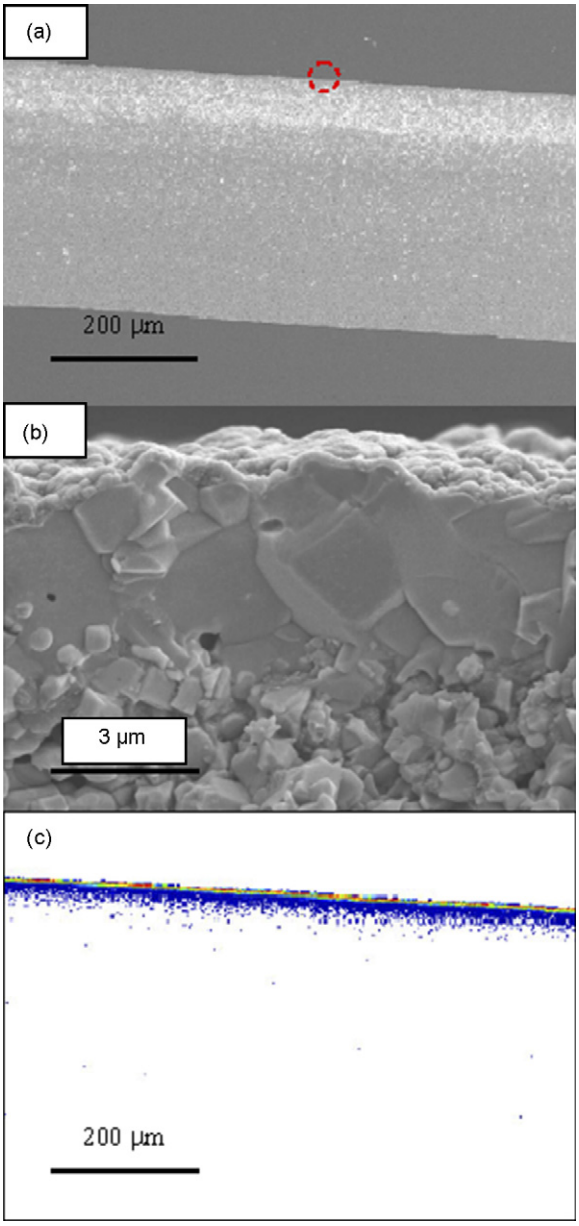


Fig. 6. Cross-section view of sintered $Li_3Fe_2(PO_4)_3$/LATP chip. (a) A SEM image, (b) an enlargement of the interface at the circle of (a) and (c) an EPMA iron map. Maximum sintering temperature was 1000 °C.

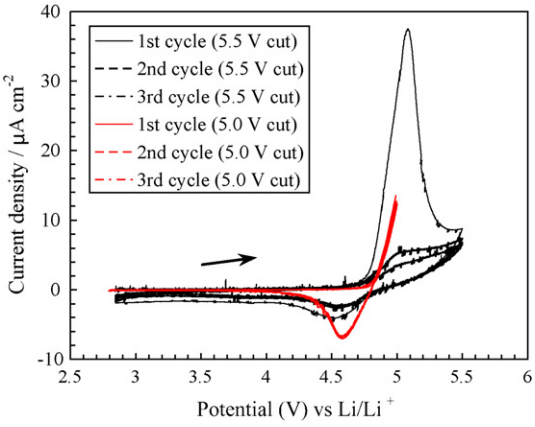


Fig. 7. Cyclic voltammograms of a model cell (Au/$LiCoPO_4$/LATP/liq. electrolyte/Li) at room temperature. Scan speed was 0.5 mV $s^{-1}$.

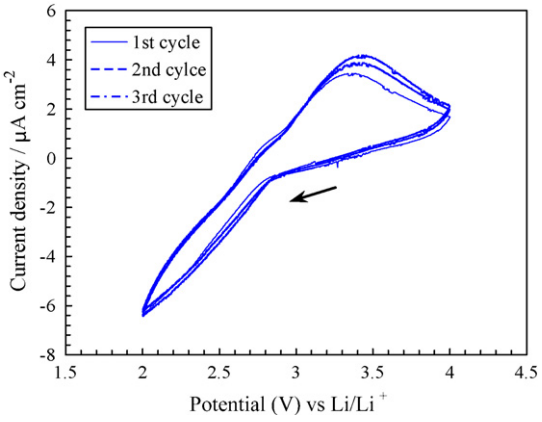


Fig. 8. Cyclic voltammograms of a model cell (Au/$Li_3Fe_2(PO_4)_3$/LATP/liq. electrolyte/Li) at room temperature. Scan speed was 0.5 mV $s^{-1}$.

$LiCoPO_4$/LATP chip, the EPMA mapping of cobalt shows that significant cobalt diffusion occurred during sintering. LATP layer with diffused cobalt was sintered well, but the opposite side of $LiCoPO_4$ showed significant porosity. The thickness of $LiCoPO_4$ was approximately 2 μm. For the $Li_3Fe_2(PO_4)_3$/LATP chip, diffusion of iron was less than cobalt. The thickness of $Li_3Fe_2(PO_4)_3$ layer was approximately 4 μm.

An electrochemical model cell was constructed with polypropylene separator, liquid electrolyte and metal lithium as a counter and reference electrode. Cyclic voltammetry was performed to evaluate the electrochemical activity of the active materials and the solid electrolyte. The results were shown in Figs. 7 and 8.

When anodic scan was performed up to 5.5 V versus $Li/Li^+$ with $LiCoPO_4$/LATP chip, a steep decrease in current was seen at 5.1 V, and only small cathodic currents were seen around 4.5 V and only small cathodic and anodic currents were seen on the following cycles. When the anodic scan was performed up to 5.0 V, the reversibility of the cyclic voltammograms were improved. These results indicate that the interface turned to be inactive when high potential over 5.0 V versus $Li/Li^+$ was applied.

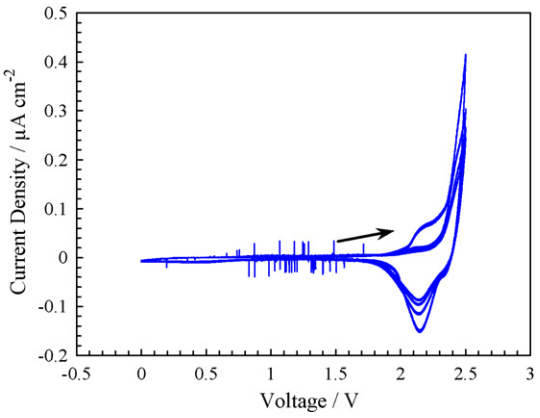


Fig. 9. Cyclic voltammograms of Au/$LiCoPO_4$/LATP/Au chip at room temperature. Scan speed was 0.5 mV $s^{-1}$.

As for a $Li_3Fe_2(PO_4)_3$/LATP chip, both cathodic and anodic currents were seen between 2.0 and 4.0 V versus $Li/Li^+$ reversibly.

These results indicate that the interface of the active material and the electrolyte constructed by sintering process was electrochemically active.

Fig. 9 shows cyclic voltammograms of $LiCoPO_4$/LATP chip and LATP was used as both a solid electrolyte and a negative electrode material. As LATP worked as an active material at around 2.5 V versus $Li/Li^+$ as shown in Fig. 7, the chip was cycled between 0 and 2.5 V. Cyclic voltammograms with fair reversibility was obtained as expected.

## 4. Conclusions

Phosphate active materials and LATP could be co-sintered without any significant side reactions. The resulted interfaces of active materials and LATP were electrochemically active. Sintering process is applicable for the construction of an all solid ceramic battery by selecting appropriate materials.

## Acknowledgements

The authors thank to K. Okano (Lighting Company, Matsushita Electric Industrial Co. Ltd.) and H. Tamai (Panasonic Electronic Devices Co. Ltd.) for fruitful discussion and experimental support.

## References

[1] K. Takada, N. Aotani, K. Iwamoto, S. Kondo, Solid State Ionics 86–88 (1996) 877.
[2] K. Hirai, M. Tatsumisago, T. Minami, Solid State Ionics 78 (1995) 269.
[3] Y. Seino, K. Takada, B.C. Kim, L. Zhang, N. Ohta, H. Wada, M. Osada, T. Sasaki, Solid State Ionics 176 (2005) 2389.
[4] R. Kanno, M. Murayama, J. Electrochem. Soc. 148 (2001) A742.
[5] J.B. Bates, N.J. Dudney, B. Neudecker, A. Ueda, C.D. Evans, Solid State Ionics 135 (2000) 33.
[6] T. Brousse, P. Fragnaud, R. Marchand, D.M. Schleich, O. Bohnke, K. West, J. Power Sources 68 (1997) 412.
[7] P. Birke, F. Salam, S. Doring, W. Weppner, Solid State Ionics 118 (1999) 149.

[8] V. Thangadurai, W. Weppner, J. Power Sources 142 (2005) 339.
[9] Y. Kobayashi, T. Takeuchi, M. Tabuchi, K. Ado, H. Kageyama, J. Power Sources 81–82 (1999) 853.
[10] H. Aono, E. Sugimoto, Y. Sadaoka, N. Imanaka, G. Adachi, J. Electrochem. Soc. 136 (1989) 590.
[11] A.K. Padhi, K.S. Nanjundaswamy, D. Masquelier, S. Okada, J.B. Goodenough, J. Electrochem. Soc. 144 (1997) 1609.
[12] K. Hirata, K. Oka, K. Komatsu, A. Nagai, US Patent 6,947,276 B2, (2005).
[13] K. Amine, H. Yasuda, M. Yamachi, Electrochem. Solid-State Lett. 3 (2000) 178.
[14] S. Patoux, C. Wurm, M. Morcrette, G. Rousse, C. Masquelier, J. Power Sources 119–121 (2003) 278.
[15] P. Maldonado-Manso, M.A.G. Aranda, S. Basque, J. Sanz, E.R. Losilla, Solid State Ionics 176 (2005) 1613.
[16] J.M. Lloris, C.P. Vincente, J.L. Tirado, Electrochem. Solid-State Lett. 5 (2002) A234.
[17] C. Masquelier, A.K. Padhi, K.S. Nanjundaswamy, J.B. Goodenough, J. Solid State Chem. 135 (1998) 228.
[18] A. Aatiq, M. Ménétrier, L. Croguennec, E. Suard, C. Delmas, J. Mater. Chem. 12 (2002) 2971.